Institute of Physics Publishing Journal of Physics: Conference Series **14** (2005) 192–205
doi:10.1088/1742-6596/14/1/023 Fourteenth International Couette Taylor Workshop

Global finite amplitude perturbations in medium aspect ratio pipe flow

F Mellibovsky and A Meseguer

Applied Physics Dept, Universitat Politècnica de Catalunya, 08034, Jordi Girona 1-3, Barcelona, Spain

E-mail: fmellibovsky@fa.upc.edu

Abstract. Results of a numerical study on the finite amplitude global perturbations inducing transition to turbulence in pipe flow are reported. The aim of this analysis is to characterise the basin of attraction of the basic *Hagen-Poiseuille* flow (which is believed to be lineary stable for all Reynolds numbers Re) by means of the minimal amplitude of an initial global perturbation triggering transition. Subcritical transition in pipe flow is extremely sensitive to the shape of the initial perturbation. The analysis is focused on the *streak breakdown* transition scenario, by which the basic flow, perturbed with streamwise-independent disturbances of azimuthal wave number $n = 1$, develops transient *streaks* that are susceptible of being destabilised by much smaller streamwise-dependent perturbations. The numerical simulations cover a wide range of Reynolds numbers $Re \in [2500, 10^4]$ and the transition dynamics are spectrally resolved by the numerical method. The threshold amplitude of perturbations seems to decrease with $Re^{-3/2}$ within the studied range.

.

1. Introduction

It has long been known that pressure-driven flow along a pipe can undergo transition to turbulence despite the linear stability of its laminar basic state (*Hagen-Poiseuille* flow) for all Reynolds numbers. However, the underlying mechanisms that govern this subcritical transition are far from being completely understood.

Since the late eighties, the stability analysis of pipe flow has been focused on the linear transient growth of small perturbations combined with nonlinear interaction as a plausible explanation for transition [1]. Non-normality of the linearised Navier-Stokes operator is responsible for substantial transient energy growth of certain perturbations. This growth has been shown to be optimal for streamwise-independent, non-axisymmetric ($n = 1$) perturbations [2]. Non-normal linear growth, combined with nonlinear saturation, leads to transient streamwise structures called *streaks*, i.e. regions where the axial flow profile exhibits strong variations and saddle points, potentially unstable with respect to three-dimensional waves of selected axial periodicity [3]. The *streak breakdown* transition scenario suggests that these 3D modes grow and trigger transition to turbulence, which is then sustained through nonlinear interaction. The transition mechanism is extremely sensitive to the shape and energy of the initial perturbation. In addition, the basin of attraction of the basic flow shrinks as Re is increased. Some unstable coherent states (travelling waves) have been identified recently, which play a key role in the sustained process of turbulence [4, 5].

The minimal amplitude of the perturbation that triggers transition as a function of Re is a way of characterising the basin of attraction of the Hagen-Poiseuille (HP) basic flow. No perturbation is capable of triggering transition below a certain value of the Reynolds number, where the basic flow is said to be unconditionally stable. Above this critical value, minimal destabilising amplitudes decrease very sharply when slightly increasing Re. For moderate and relatively high values of the Reynolds number, it is believed that the threshold amplitude, A_{cr}, decays as a power law of Re ($A_{cr} \sim Re^{\gamma}$), whose critical exponent γ has been object of controversy. The critical Re together with the minimal amplitude curve are known as the *double threshold* [6]. Recent experimental and numerical studies[7, 5, 4] reveal a value of $\gamma \approx -1$, whereas former experimental analyses [8] and low dimensional numerical simulations [9] predicted a slightly lower exponent of $\gamma \approx -3/2$.

A spectral solenoidal Petrov-Galerkin code has been developed and validated in order to simulate the evolution of perturbations in HP flow. It is not the aim of this code to resolve fully developed turbulent motion. The intention here is to give an accurate picture of the initial stages of transition. The time integrations are carried out with medium-high spatial resolutions (equivalent to a collocation mesh of 33 nodes in the axial, azimuthal and radial coordinates) on a pipe up to 20 diameters long. The perturbations to the basic flow chosen as initial condition consist of finite amplitude streamwise vortices of selected azimuthal symmetry, on top of which 3D modulation of selected axial periodicity and much smaller size are added. The study covers a range of Re from 2500 to 10000. These simulations seem to confirm the $-3/2$ value for the exponent γ.

The paper is structured as follows. In section §2 we formulate the problem mathematically and give an outline of the numerical method used to solve it. Section §3 introduces the *streak breakdown* transition mechanism and illustrates it with an example. The global perturbations used throughout the study are characterised in section §4. At this point, the stage is set for a vast exploration, the results of which are detailed in section §5. We discuss these results in section §6, to finally extract some conclusions in section §7.

2. Mathematical formulation and numerical approach

In the present study, the fluid is assumed to be incompressible (density ρ) and viscous (kinematic viscosity ν). The fluid is driven through a cylinder of radius a by a pressure gradient Π_0 pointing in the direction of the cylinder axis. The fluid motion is governed by the incompressible Navier-Stokes equations

$$\partial_t \mathbf{v} + (\mathbf{v}\cdot\nabla)\mathbf{v} = -\frac{\Pi_0}{\rho}\hat{\mathbf{z}} - \nabla p + \nu\Delta\mathbf{v}, \tag{1}$$

$$\nabla\cdot\mathbf{v} = 0, \tag{2}$$

where $\mathbf{v}$ is the velocity vector field, which satisfies non-slip boundary condition on the wall

$$\mathbf{v}_{wall} = \mathbf{0}, \tag{3}$$

and p is the reduced pressure.

The problem is most easily formulated in cylindrical coordinates, due to the geometry of the domain. Therefore, the velocity field is given in terms of its radial ($\hat{\mathbf{r}}$), azimuthal ($\hat{\theta}$) and axial ($\hat{\mathbf{z}}$) components

$$\mathbf{v} = u\,\hat{\mathbf{r}} + v\,\hat{\theta} + w\,\hat{\mathbf{z}} = (u, v, w), \tag{4}$$

where u, v and w are functions of the three spatial coordinates (r, θ, z) and time t. Equations (1) and (2), subject to the boundary condition (3), admit an analytical steady solution by the

name of *Hagen-Poiseuille flow* that reads

$$\mathbf{v}_{\mathrm{B}} = (u_{\mathrm{B}}, v_{\mathrm{B}}, w_{\mathrm{B}}) = \left(0\ ,\ 0\ ,\ -\frac{\Pi_0 a^2}{4\rho\nu}\left[1 - \left(\frac{r}{a}\right)^2\right]\right), \quad p_{\mathrm{B}} = C, \tag{5}$$

where C is an arbitrary constant. This solution corresponds to an axisymmetric streamwise-independent parabolic purely-axial velocity profile, depending only on the radial coordinate. The velocity attains its maximum $U_{\mathrm{CL}} = -\Pi_0 a^2/4\rho\nu$ at the pipe axis. All variables of the problem can be rendered non-dimensional using a and U_{CL} as the length and velocity scales, respectively. The advective time, defined as $\tau = a/U_{\mathrm{CL}}$, is used as the time scale to non-dimensionalise the equations. After non-dimensionalisation, the basic flow takes the form

$$\mathbf{v}_{\mathrm{B}} = (u_{\mathrm{B}}, v_{\mathrm{B}}, w_{\mathrm{B}}) = (0\ ,\ 0\ ,\ 1 - r^2), \tag{6}$$

and the dynamics are governed by the *Reynolds number* (Re):

$$Re = \frac{a\, U_{\mathrm{CL}}}{\nu}. \tag{7}$$

The velocity and pressure fields can be decomposed in the basic solution plus an additive perturbation:

$$\mathbf{v}(r,\theta,z,t) = \mathbf{v}_{\mathrm{B}}(r) + \mathbf{u}(r,\theta,z,t), \tag{8}$$

$$p(r,\theta,z,t) = p_{\mathrm{B}} + q(r,\theta,z,t). \tag{9}$$

Substitution of (8) and (9) in the non-dimensional version of (1) and (2) yields the governing equations for the perturbation:

$$\partial_t \mathbf{u} = -\nabla q + \frac{1}{Re} - (\mathbf{v}_{\mathrm{B}} \cdot \nabla)\mathbf{u} - (\mathbf{u} \cdot \nabla)\mathbf{v}_{\mathrm{B}} - (\mathbf{u} \cdot \nabla)\mathbf{u}, \tag{10}$$

$$\nabla \cdot \mathbf{u} = 0. \tag{11}$$

We will assume periodic boundary condition in the axial coordinate. The problem is then solved in the spatial domain

$$\Omega = \{(r,\theta,z) \mid 0 \le r \le 1,\ 0 \le \theta < 2\pi,\ 0 \le z < Q\}, \tag{12}$$

Q being the dimensionless length of the pipe in radius units.

The velocity field must satisfy the non-slip boundary condition at the wall and periodicity in the axial and azimuthal directions:

$$\mathbf{u}(1,\theta,z,t) = 0, \tag{13}$$

$$\mathbf{u}(r,\theta + 2\pi n, z, t) = \mathbf{u}(r,\theta,z,t), \tag{14}$$

$$\mathbf{u}(r,\theta,z + Ql, t) = \mathbf{u}(r,\theta,z,t), \tag{15}$$

for $(n,l) \in \mathbb{Z}^2$, $(r,\theta,z) \in [0,1] \times [0,2\pi) \times [0,Q)$, and $t > 0$. To fully determine the solution, an initial condition must be prescribed:

$$\mathbf{u}(r,\theta,z,0) = \mathbf{u}_0, \tag{16}$$

where $\mathbf{u}_0$ is a divergence-free vector field satisfying the boundary conditions.

The spatial discretisation of equation (10) is implemented with a solenoidal Petrov-Galerkin spectral method. Velocity $\mathbf{u}$ is replaced by its expansion in a basis of solenoidal

analytical functions satisfying the periodicity and boundary conditions. Analyticity of the approximation to overcome the singularity of polar coordinates at the origin is accomplished by the regularisation rules proposed in former works [10]. Fourier expansions are naturally used in the azimuthal and axial directions, while Chebyshev-based functions are more suitable for the radial coordinate. The expansion is truncated at order L in z, order N in θ and order M in r:

$$\mathbf{u}(r,\theta,z,t) = \sum_{l=-L}^{L}\sum_{n=-N}^{N}\sum_{m=0}^{M} a_{lnm}(t)\mathbf{\Phi}_{lnm}(r,\theta,z), \tag{17}$$

$$\mathbf{\Phi}_{lnm}(r,\theta,z) = \mathrm{e}^{\mathrm{i}(2\pi lz/Q+n\theta)}\mathbf{v}_{lnm}(r). \tag{18}$$

The velocity field associated with the axial-azimuthal Fourier mode (l,n) is defined as follows:

$$\mathbf{u}_{ln}(r,\theta,z,t) = \sum_{m=0}^{M} a_{lnm}(t)\mathbf{\Phi}_{lnm}(r,\theta,z). \tag{19}$$

The spatial discretisation is accomplished by formal substitution of expansion (17) in equation (10) and projection over another set of solenoidal fields [11, 12]. The projection of the nonlinear advective term is computed with a pseudospectral method de-alising in θ and z using the 3/2-rule [13]. The resulting ODE system for the amplitudes is discretised in time by means of an implicit 4^{th}-order BDF method suitably combined with an explicit 4^{th}-order modified Adams-Bashforth [14]. The iteration process is started with a 4^{th}-order Runge-Kutta method [15].

3. Streak Breakdown

Even though the basic flow is linearly stable (any perturbation must decay exponentially), non-normality of the linearised Navier-Stokes operator is responsible for the significant transient growth of some disturbances. The maximum linear amplification has been shown to occur for streamwise-independent modes of azimuthal wave number $n = 1$ [2]. Disturbances mainly exciting these highly amplified modes, develop into streamwise-independent (two-dimensional, 2D) structures called *streaks*. These 2D structures, happen to exhibit inflectional velocity profiles, which make them unstable, in a transient sense, to three-dimensional (3D) perturbations of selected axial periodicity that might be present in the flow. In the presence of the *streaks*, these 3D perturbations grow exponentially, eventually leading to turbulence provided that they have reached high enough energy level by the time the *streaks* start to decay due to viscosity. Zikanov investigated the stability of the *streaks* by linearising the 2D-*streaks* modulated flow as a function of time [3]. This allowed to single out the 3D perturbations that undergo the largest growth in the presence of the *streaks*. The axial wave number (κ) of the most amplified 3D perturbation was found as a function of Re and of the initial energy (ϵ^0_{2D}) of the 2D perturbation. As an example, a 3D perturbation with $\kappa \sim 1.5$ was found to be the most amplified in the presence of *streaks* generated from a 2D perturbation of energy $\epsilon^0_{2D} = 10^{-2}$ at $Re = 3000$.

A natural definition for the energy of an arbitrary vector field u is

$$\mathrm{E}(\mathbf{u}) = \frac{1}{2}\int_0^Q \mathrm{d}z \int_0^{2\pi} \mathrm{d}\theta \int_0^1 r\mathrm{d}r\ \mathbf{u}^*\cdot\mathbf{u}. \tag{20}$$

Using this definition, the energy of the *Hagen-Poiseuille* flow (E_{HP}) can be computed analytically and used to normalise the energy of any perturbation velocity field:

$$\epsilon(\mathbf{u}) = \frac{\mathrm{E}(\mathbf{u})}{\mathrm{E}_{HP}}, \quad \mathrm{E}_{HP} = \frac{\pi Q}{6}. \tag{21}$$

Due to the orthogonality of the Fourier system, the energy of the velocity field can be written as:

$$\epsilon(\mathbf{u}) = \sum_{l=-L}^{L} \sum_{n=-N}^{N} \epsilon_{ln}, \tag{22}$$

where $\epsilon_{ln} = \epsilon(\mathbf{u}_{ln})$ is the normalised energy of the velocity field associated to the pair (l, n) defined in (19). Therefore, the energy of the *streaks* can be interpreted as the total energy of all the streamwise-independent modes, since they are an invariant solution of the *Navier-Stokes* equation, due to the axial nature (symmetry properties) of the basic flow. As a result, the energy associated with the 2D perturbation is

$$\epsilon_{2D} = \sum_{n=-N}^{N} \epsilon_{0n}. \tag{23}$$

To illustrate the formation of the *streaks*, a purely 2D run (with resolution $N = 15$, $M = 25$, equivalent to a collocation mesh of $M_r \times N_\theta \times L_z = 26 \times 31 \times 1$ points, and $\Delta t = 0.01$) at $Re = 3000$, gives a clear example. The initial perturbation excites an $n = 1$ azimuthal mode:

$$\mathbf{u}_0 = \mathbf{u}^0_{2D} = A_{2D}\, \mathrm{e}^{\mathrm{i}\theta}\ (-\mathrm{i}f_1(r), f_2(r), 0) + \text{c.c.}, \tag{24}$$

where $f_1(r) = 1 - 2r^2 + r^4$, $f_2(r) = 1 - 6r^2 + 5r^4$, c.c. stands for complex conjugate and A_{2D} is determined so that $\epsilon(\mathbf{u}^0_{2D}) = \epsilon^0_{2D} = 10^{-2}$.

Figure 1 shows the time evolution of the energy associated with the 2D perturbation, in very good agreement with Zikanov's results and with previous computations at much lower spatial resolution with the same method provided by Meseguer [3, 9]. The axial velocity distribution on a cross-section of the pipe, shown in figure 2, is also coincident with that obtained in these previous studies. The cross-sectional axial velocity distribution has been represented at several times to sketch the development of the *streaks* in the absence of 3D perturbations.

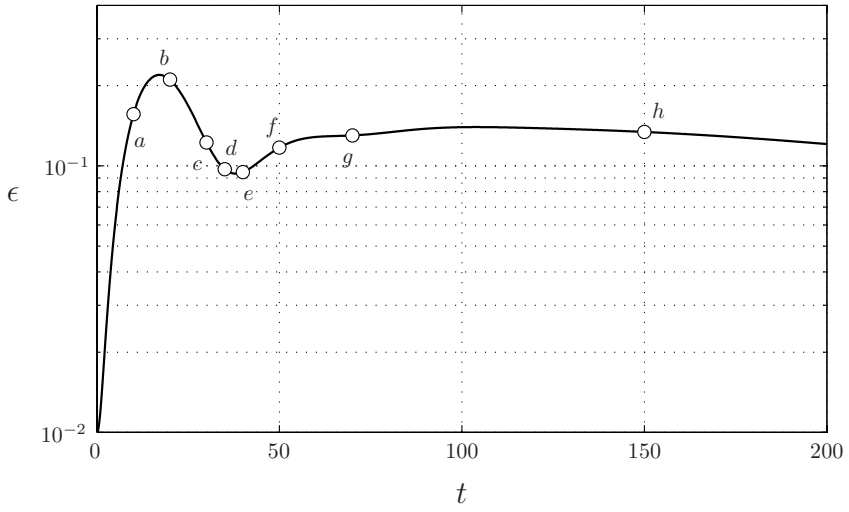

Figure 1. Time evolution of the energy of the *streaks* developing from the 2D perturbation prescribed in equation (24), for $Re = 3000$.

In order to obtain a *streak breakdown*, 3D perturbations of a suitable axial periodicity must be added to the 2D perturbation. The new initial condition is:

$$\mathbf{u}_0 = \mathbf{u}^0_{2D} + \mathbf{u}^0_{3D}, \tag{25}$$

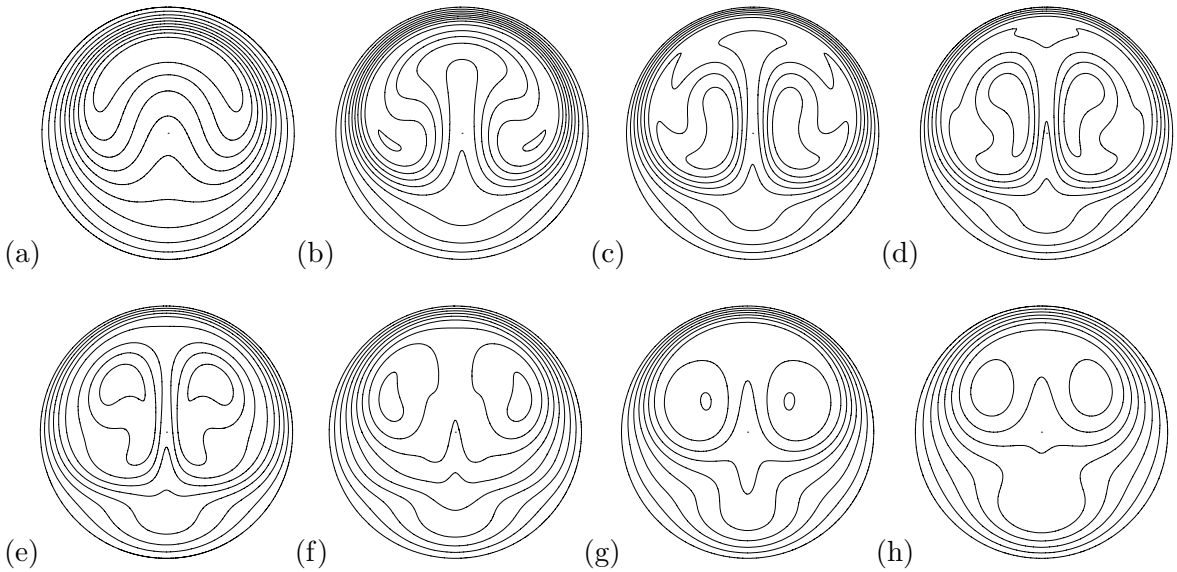

Figure 2. Axial velocity contours on a cross-section corresponding to the time integration plotted in figure 1, $\epsilon^0_{2D} = 10^{-2}$. Snapshots are taken at times a) $t = 10$, b) $t = 20$, c) $t = 30$, d) $t = 35$, e) $t = 40$, f) $t = 50$, g) $t = 70$ and h) $t = 150$.

where $\mathbf{u}^0_{2D}$ is the same 2D perturbation described in (24), and $\mathbf{u}^0_{3D}$ is a 3D perturbation of the form

$$\mathbf{u}^0_{3D} = \sum_{n=-4}^{4} A^n_{3D}\mathbf{v}_n \quad + \text{c.c.}, \tag{26}$$

with

$$\mathbf{v}_n = \begin{cases} \mathrm{e}^{\mathrm{i}\kappa z}\ (0, f_3(r), 0) & n = 0 \\ \mathrm{e}^{\mathrm{i}(\kappa z + n\theta)}\ (-\mathrm{i}n f_1(r), f_2(r), 0) & n \neq 0, \end{cases} \tag{27}$$

where $f_3(r) = r(1 - r^2)$.

As a result, nine azimuthal modes, with $|n| \leq 4$, and the same axial wave number $\kappa = 1.67$ (close to the optimal of 1.5, according to Zikanov's results at $Re = 3000$ for a 2D perturbation of initial energy $\epsilon^0_{2D} = 10^{-2}$), constitute the initial 3D perturbation ($\mathbf{u}^0_{3D}$), which is added to the same 2D perturbation ($\mathbf{u}^0_{2D}$) as before. The amplitudes A^n_{3D} are chosen so that the initial 3D energy $\epsilon^0_{3D} = 9 \cdot 10^{-9}$ is uniformly distributed among the 3D modes.

The resolution for the 3D run has been set to $L = 15$, $N = 15$, $M = 25$ ($M_r \times N_\theta \times L_z = 26 \times 31 \times 31$) and $\Delta t = 0.01$, with $Q \simeq 20$, so the maximum axial wave number is $\kappa_{max} = 5$.

In order to see the time-signature of the *streaks* and their breakdown as the 3D perturbations grow, the quantity $\epsilon_{2D}(t)$ as defined in (23) is not well suited. Interpretation of the energy of the streamwise-independent axisymmetric Fourier mode $(n, l) = (0, 0)$, included in (23), is misleading, since it is strongly coupled with axisymmetric modes of any axial periodicity, like the one with $\kappa = 1.67$ excited by the 3D perturbation. Turbulence redistributes energy via non-linear mixing, transfering energy from all axial and azimuthal modes to the $(n, l) = (0, 0)$-mode. Hence, it is better to define the energy of the *streaks* as

$$\epsilon_{streaks}(t) = \sum_{|n|=1}^{N} \epsilon_{0n}(t), \tag{28}$$

in order to better capture their energy loss in the presence of the 3D perturbation. To evidence the *streak breakdown* process, it seems natural to compute the energy of the 3D perturbation as

the sum of the energies of all the azimuthal modes with $\kappa = 1.67$, not paying much attention to modes with neighbouring κ's or its harmonics, excited through non-linear interaction. To this purpose, we define the energy associated to the optimal destabilised 3D perturbation as

$$\epsilon_{3D}(t) = \sum_{n=-N}^{N} \epsilon_{5n}(t), \tag{29}$$

where $l = 5$ corresponds to $\kappa = 1.67$.

Results are shown in figure 3. The bold continuous line represents the energy of the *streaks* $\epsilon_{streaks}$, while the thin line corresponds to the energy of the 3D perturbation ϵ_{3D}. The energy of the unperturbed *streaks* resulting from the purely 2D run ($\epsilon^{2D}_{streaks}$) has also been plotted (dashed line) for comparison. The *streaks* energy loss with respect to the unperturbed *streaks* as the 3D perturbation grows, confirms the *streak breakdown* mechanism. Figure 4 features the cross-

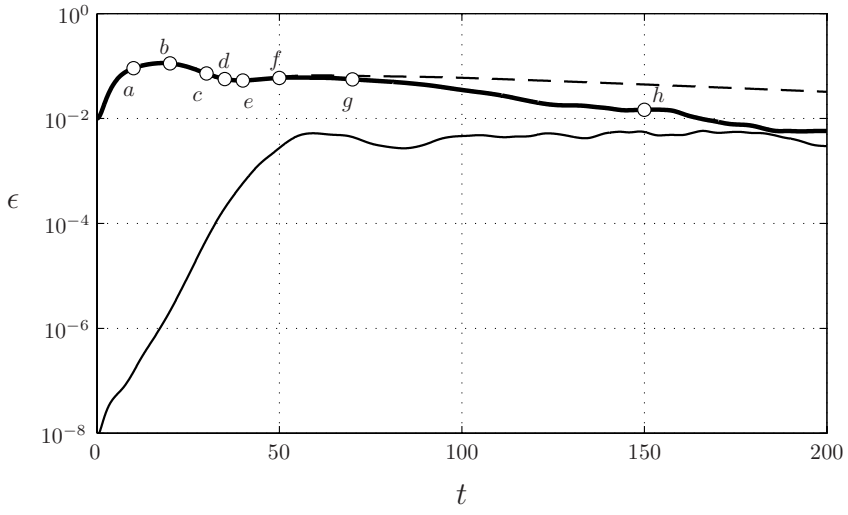

Figure 3. Time evolution of the energy of the *streaks* (bold line) and of the 3D perturbation (thin line) developing from the initial disturbance described in equation (26) for $Re = 3000$. The energy of the unperturbed *streaks* in figure 1 has also been represented (dashed line) to allow comparison.

sectional axial-velocity contours of the 3D run at the same times as in figure 3. The velocity profile is the same (to plotting accuracy) for both simulations up to $t = 35$, when the *streaks* are already established. From this point on, while the 2D run shows the ensuing evolution of the *streaks*, in the 3D runs we attend to their destabilisation ($t = 50$) and subsequent breakdown into a completely unstructured flow ($t = 150$).

4. Characterisation of global perturbations

Even though the *HP* flow is linearly stable for all values of Re, it is unconditionally stable for small values only. Beyond this lower critical Reynolds number within the range $Re \in [1760, 2300]$, finite amplitude perturbations capable of inducing permanent turbulence exist. It is a well known fact that the critical amplitude of the perturbation that makes the flow depart from laminarity diminishes when increasing Re. The most accurate experiments have been able to maintain laminarity up to $Re = 10^5$ [16].

From the point of view of a dynamical system, this may be suggesting that unstable states bifurcate from branches not connected with the *HP* solution, thus bounding its basin of attraction. Perturbations leaving the flow out of this basin, would be captured by this unstable states leading to turbulence. Some of such coherent states (travelling waves) have been recently found [4, 5] though their role in inducing turbulence, albeit suspected crucial, is not clear yet.

The main goal of this work is to study the topological structure of the basin of attraction of the basic regime. A way of doing so is by finding, as a function of Re, the minimal amplitude of

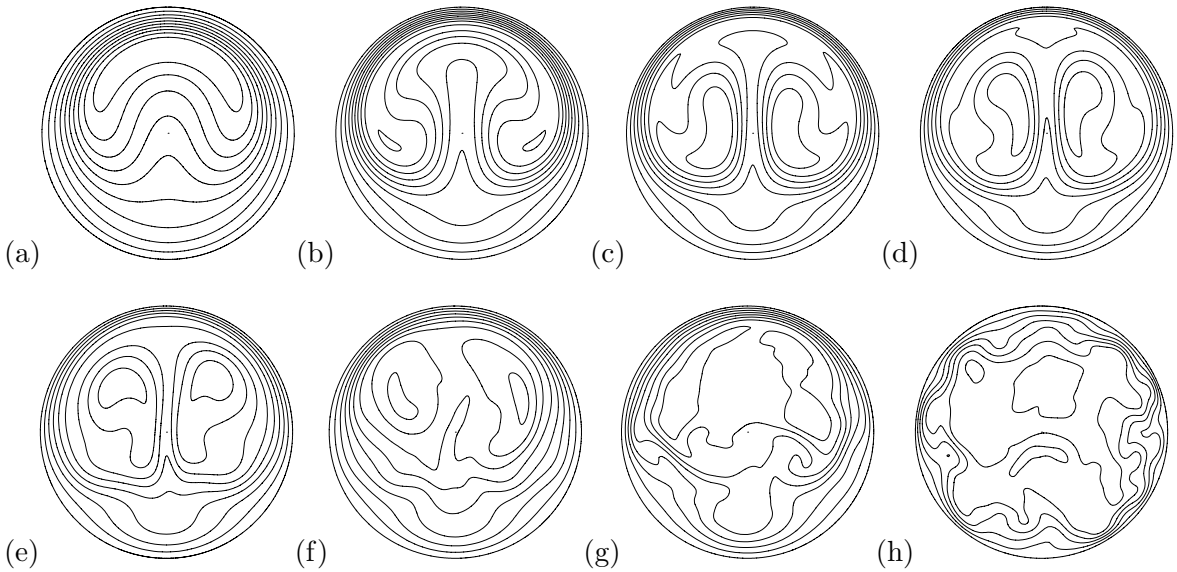

Figure 4. Axial velocity contours on a cross-section corresponding to the points marked in figure 3. Snapshots are taken at the same times as in figure 2.

a perturbation capable of triggering transition. Any perturbation ($\mathbf{u}$) can be expressed in terms of its normalised energy, $\epsilon(\mathbf{u})$, and of its modal distribution or perturbation shape $\hat{\mathbf{u}}$,

$$\mathbf{u} = \epsilon(\mathbf{u})\ \hat{\mathbf{u}}. \tag{30}$$

The critical amplitude is then defined as

$$A_{cr} = \sqrt{\epsilon_{cr}}, \tag{31}$$

where ϵ_{cr} is the minimum energy associated with the most efficient shape, among all possible modal distributions. To properly find $A_{cr}(Re)$, a three-fold parametric study would be required, exploring all relevant Re and perturbation shapes (axial and azimuthal wave numbers l and n, and radial profiles), and testing as many perturbation energies (ϵ^0) as necessary to bound criticality. The limiting factor of such a study is the existence of an infinity of possible perturbation shapes. Although the number of possible modal energy distributions becomes finite once the problem has been discretised, searching for the optimal shape is not feasible, even for coarse grained computations. Instead, reviewing results from previous parametric studies and making some additional assumptions, it appears reasonable to fix the shape of what seems to be a nearly optimal perturbation (optimal in the sense of its ability to trigger transition with minimal initial energy) and proceed to sweep the two remaining parameters.

We will restrict our study to the *streak breakdown* scenario, presented in section §3, which has been proved to be utterly effective in triggering transition. According to Zikanov's work, the optimal perturbation at $Re = 3000$, in the presence of *streaks* originated from an initial 2D perturbation of energy $\epsilon^0_{2D} = 10^{-2}$, must excite modes with $\kappa \sim 1.5$. Since the critical threshold at this Re happens to be located at about this energy value, the optimal perturbation can be directly deduced from this result. Nothing can be said, however, about the critical perturbation at higher Re. Zikanov's analysis elucidates which value of κ is most amplified at $Re = 3000$ as a function of ϵ^0_{2D}, and what the effect is of increasing Re at a given ϵ^0_{2D} for the optimal κ's at $Re = 3000$. The effect of increasing Re, combined with a reduction of ϵ^0_{2D} has not been examined. This combination is crucial to tracking the critical amplitude threshold. Some prospective runs

with the fully non-linear code at high Re seem to suggest that the optimal κ is the same or slightly higher in the proximity of the transition threshold. The aforementioned correlations are summed up as follows:

$$\begin{cases} A_{cr} = \min_\kappa \widehat{A}_{cr}(Re,\kappa) = \widehat{A}_{cr}(Re,\kappa_{opt}) \\ \kappa_{opt} = \kappa_{opt}(Re,A) \end{cases} \tag{32}$$

where $\widehat{A}_{cr}$ is the critical amplitude of a perturbation exciting axial wave number κ. A_{cr} can only be obtained after an iterative process, as it depends on κ_{opt}, which in turn depends on A.

Bearing all these results in mind, the initial perturbation for all runs is chosen to be composed of a two-dimensional streamwise-independent non-axisymmetric (2D) perturbation with azimuthal wave number $n = 1$ plus a streamwise-dependent three-dimensional (3D) perturbation exciting axial wave numbers in the range $\kappa \in [1.5, 2.2]$. The azimuthal wave number of this latter component of the perturbation is chosen to be $n = 0, \pm 1$, since some energy-field plots from Zikanov's study reveals a predominance of this kind of symmetry. The bulk of the initial energy is then assigned to the 2D component of the perturbation (ϵ^0_{2D}) while the 3D component takes only $\epsilon^0_{3D} = 9 \cdot 10^{-8}$, evenly distributed among several modes ($n = 0, \pm 1$, $\kappa = 1.5625, 1.875, 2.1875$). The amplitude of the perturbation is defined as

$$A = \sqrt{\epsilon_{2D} + \epsilon_{3D}} \simeq \sqrt{\epsilon_{2D}}. \tag{33}$$

Regarding the radial profile of the perturbation, only the simplest distribution of velocities compatible with the divergence-free and boundary conditions is used. The resulting perturbation is analogous to that described in (24), with the only exception that the 3D component excites modes with $n = 0, \pm 1$ and $\kappa = 1.5625, 1.875, 2.1875$, instead of $|n| \leq 4$ and $\kappa = 1.67$.

The resolution for the simulations has been set to $L = 16$, $N = 16$ and $M = 24$ ($M_r \times N_\theta \times L_z = 25 \times 33 \times 33$) for a vast exploration, then increased to $L = 16$, $N = 16$ and $M = 32$ ($M_r \times N_\theta \times L_z = 33 \times 33 \times 33$) for further refinements intended to accurately capture the critical amplitude threshold. No substantial differences have been observed when increasing the resolution. The maximum axial wave number has been set to $\kappa_{max} = 5$. These values correspond to a medium pipe length of $Q = 2\pi L/\kappa_{max} \simeq 20$ pipe radii. The choice of these values for the parameters implies some compromises. First, the radial resolution M is conditioned by the maximum axial wave number κ_{max}, since an increasing number of Chebyshev modes is necessary to properly resolve the eigenspectrum of the linearised Navier-Stokes operator. Second, it is interesting to have κ_{max} much bigger than that of most rapidly growing three-dimensional perturbations in the presence of *streaks* in order to capture some of the harmonics. And third, a big κ_{max} takes many axial modes L to represent a long pipe, which is crucial to capturing long axial wavelength phenomena.

The perturbation to the basic flow constitutes therefore a global disturbance and is applied as an initial condition of the form

$$\mathbf{u}_0 = \mathbf{u}^0_{2D} + \mathbf{u}^0_{3D}, \tag{34}$$

with

$$\mathbf{u}^0_{2D} = A_{2D}\, \mathrm{e}^{\mathrm{i}\theta}\ (-\mathrm{i}f_1(r), f_2(r), 0)\ + \text{c.c.}, \tag{35}$$

and

$$\mathbf{u}^0_{3D} = \sum_{l=5,6,7} \sum_{n=0,\pm 1} A^{ln}_{3D} \mathbf{v}_{ln}\ + \text{c.c.}, \tag{36}$$

where the fields $\mathbf{v}_{ln}$ are

$$\mathbf{v}_{ln} = \begin{cases} \mathrm{e}^{\mathrm{i}\frac{2\pi}{Q}lz}\ (0, f_3(r), 0) & n = 0 \\ \mathrm{e}^{\mathrm{i}(\frac{2\pi}{Q}lz + n\theta)}\ (-\mathrm{i}nf_1(r), f_2(r), 0) & n \neq 0. \end{cases} \tag{37}$$

For the simulation parameters stated, modes $l = 5, 6, 7$ in equation (36) correspond to axial wave numbers $\kappa = 1.5625, 1.875, 2.1875$, respectively. A_{2D} is chosen so that $\epsilon(\mathbf{u}^0_{2D}) = \epsilon^0_{2D}$, and the coefficients A^{ln}_{3D} are taken to uniformly distribute an initial energy ϵ_{3D} among the 3D modes.

5. Basin of attraction of the basic flow: results

A first exploration has been carried out with the lower spatial resolution, exploring the range $Re \in [2500, 10^4]$ for widely spread initial perturbations amplitudes ($10^{-2} \lesssim \epsilon \lesssim 10^{-1}$), in order to roughly approximate the critical threshold. A second set of runs with the higher resolution has then been performed to better describe the critical curve and to extend it up to $Re = 12600$.

It is necessary at this point, to establish a set of criteria to help decide on whether a point corresponds to a transitional run or not. It is crucial to run up to a *time-horizon* at which the *streaks* have fully developed and the 3D perturbations have had enough time to grow. This time has been found to be of at least $T = 1000$ advective time units for the lowest ϵ_{2D} at the highest Re explored. However, for $Re < 7500$, $T = 600$ has been proven enough. Experimentally, considering the perturbation is at worst advected downstream at the basic flow maximum axial speed, this is equivalent to having the observation point at 300 to 500 diameters distance downstream from the perturbation point. The longest constant mass flow rig used in experiments allows to make observations up to 530 diameters downstream from the perturbation location [7], which our time-horizons represent well enough. Checking for turbulence after this time is therefore a reasonable approach, and this is done by a bare eye inspection of the modal energy distribution. A simulation run is considered *turbulent* if the energy associated to the excited 3D modes remains three orders of magnitude above its initial level for $t \geq T$, evolving in a chaotic way, and the energy of the 2D mode has fallen to the same order of magnitude than that of the 3D modes (implying that the *streaks* have been broken). This is summarised as follows:

$$\epsilon_{3D}(T) \geq 10^3 \, \epsilon_{3D}(0), \tag{38}$$

and

$$O(\epsilon_{2D}(T)) \sim O(\epsilon_{3D}(T)), \tag{39}$$

for a *turbulent* run, otherwise *laminar*.

For low Re, however, transition for a limited time-window with an eventual relaminarisation has been consistently observed. These runs would have appeared as turbulent depending on the position of the observation area in an experimental rig. We will label these runs as *relaminarised*, separating them from *turbulent* and *laminar* runs. The existence of this phenomenon suggests that some of the runs considered turbulent within a time-horizon of $T = 600$ may have relaminarised if longer runs had been envisaged.

Figures 5a, 5b and 5c illustrate a *laminar*, a *turbulent* and a *relaminarised* run, showing the time evolution of the energy of the modes excited by the initial perturbation. The bold line starting at a higher energy level corresponds to the energy of the mode excited by the 2D perturbation ($n = 1$ and $\kappa = 0$), which constitutes a reliable signature of the development of the *streaks*. The other 9 thin lines are the energies of the modes directly excited by the 3D perturbation ($n = 0, \pm 1$ and $\kappa = 1.5625, 1.875, 2.1875$). From figures like 5a, 5b and 5c, it can be concluded whether the flow is laminar or turbulent by looking at the regular or chaotic evolution of the energies.

The differences among the three runs are clearly visible in the examples plotted. In the case of the *laminar* run (figure 5a), the 3D perturbation is only temporarily excited once the *streaks* have developed. Nonetheless, this tendency is soon reverted and their energy rapidly decays before having been able to perturb the streamwise *streaks*. The initial response of the energies in the case of the *turbulent* run (figure 5b) is completely analogous. It differs from the *laminar* run only in that the 3D perturbation manages to grow fast enough in the presence of the *streaks*

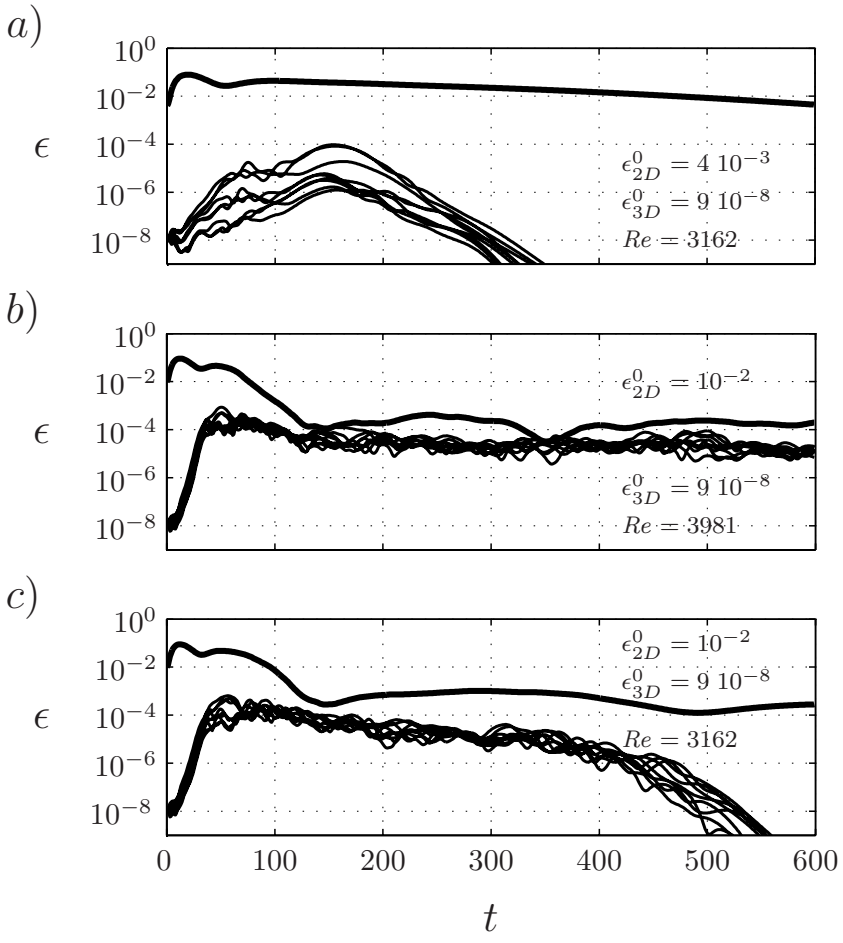

Figure 5. Time evolution of the energies of the 2D mode (bold line) and of the 3D modes (thin lines) corresponding to **a)** *laminar*, **b)** *turbulent* and **c)** *relaminarised* simulations. In all three cases, the spectral resolution has been fixed to $M_r \times N_\theta \times L_z = 25 \times 33 \times 33$.

to actually break them and set off the peculiar chaotic dynamics of turbulent motion. This *streak breakdown* can be spotted on the 2D mode energy, which parts from the evolution it would have had in a purely two-dimensional run. The only difference with the *relaminarised* run (figure 5c), is that the new dynamics are sustained for the whole run, while for the latter, the turbulent motion is abruptly interrupted and the energy of the 3D modes start decaying rapidly whilst the *streaks* recover temporarily to slowly vanish afterwards.

The results of the coarse exploration, classified according to the criteria detailed above, are shown in figure 6. White triangles ($\bigtriangledown$) represent *laminar* runs, black circles ($\bullet$) denote *turbulent* runs and empty circles ($\circ$) correspond to *relaminarised* runs (i.e., runs for which transition is observed, but followed by relaminarisation). The critical amplitudes, obtained from the refined exploration, have been marked with crosses ($\times$). It is remarkable how relaminarisation is very common at low Re, where the *HP* flow preserves sound stability properties and considerably big perturbations are required to trigger transition. As expected, A_{cr} is a decreasing function of Re. In fact, the double threshold $Re_{cr} - A_{cr}(Re)$ is evidenced by the behaviour of the slope, very pronounced at low Re (allegedly converging to a vertical asymptote at Re_{cr}), and getting milder as Re increases. The region marked in figure 6 with a square has been zoomed on in figure 7.

It is believed that the minimum destabilising amplitude decreases as a power of Re for Re tending to infinity ($A_{cr} \sim Re^{\gamma}$). This has been formally proved to be the case in plane channel flows such as plane Poiseuille and plane Couette, for which the asymptotic exponent has been shown to be $\gamma = -3/2$ and $\gamma = -1$, respectively [17]. This behaviour would appear in a log-log

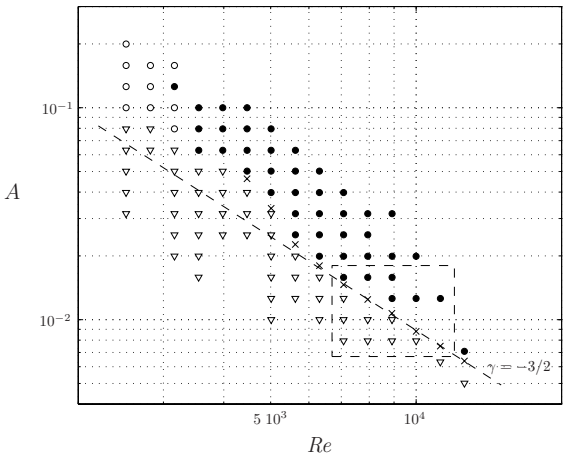

Figure 6. A vs Re, containing the results from the coarse exploration. *Laminar* ($\triangledown$), *turbulent* ($\bullet$) and *relaminarised* ($\circ$) simulations are represented. The critical amplitudes resulting from the refined exploration are also marked ($\times$).

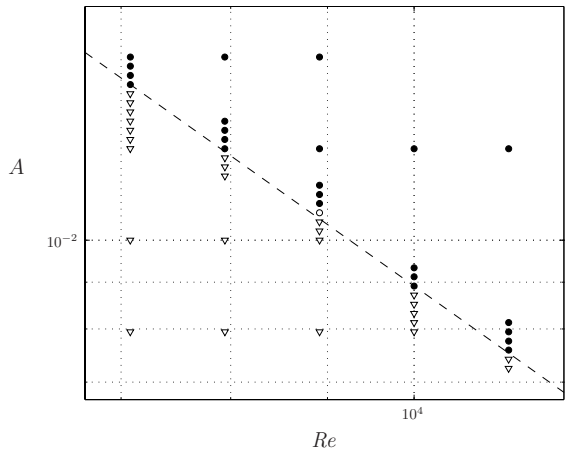

Figure 7. Zoom on the square box in figure 6. All simulations (coarse and fine) are represented. The symbols retain the same meaning as in figure 6.

plot as a straight line of slope γ, and this is exactly what the critical threshold line seems to converge to towards the right side of the plot. These numerical experiments suggest that pipe Poiseuille flow follows the same behaviour as other shear flows with a slope $\gamma = -3/2$, at least within the studied range.

6. Discussion

In contrast with this result, some numerical studies [5, 4, 20], seem to be consistent with the experimental value of -1 recently obtained in a constant mass flux long pipe [7]. We claim that the origin of the discrepancy can be ascribed to differences in the problem formulation. The present study concentrates on an initial condition problem, leaving a global perturbation on the basic flow free to evolve and either develop into turbulence or eventually decay. The focus is, then, on the amplitude of the minimal initial global perturbation capable of sparking transition. Instead, the experimental setup deals with local perturbations violating the boundary conditions (fluid is injected) and which are extended in time. Furthermore, the perturbation is structuraly rigid in the sense that its shape cannot be modified at will. The 6-jets oblique injection used by Hof, Juel & Mullin in their experiments mainly excites azimuthal modes with $n = 3$ and high axial modes, that have been proved to be not optimal, according to the present computations.

Another point of concern is the definition of perturbation amplitude, which is very naturally based on energy considerations in our numerical runs, while somewhat confusing in experiments, where it is merely based on the injection to total pipe mass flow ratio, regardless of the overall duration of the injection. Some attempts have been made [18] to relate the amplitude definition used in several experimental [19, 8] and theoretical [17] studies. In any case, it is remarkably astonishing that the experiments find the asymptotic behaviour from Re as low as 2000.

With regard to the recent numerical study [4], from which a $\gamma = -1$ can be deduced, although not explicitly computed, significant differences make it difficult to compare with our own results. The main differences concern the initial perturbation shape, which Faisst and Eckardt generate randomly. This sets the stage for an *oblique transition* rather than the *streak breakdown* scenario we have adopted. Although their results are very valuable for a statistical analysis of transition,

the fact that energy may be wasted on irrelevant modes, together with the low Re to which their simulation runs correspond, make their results not readily comparable to ours. Another computational study [20] explores the linear stability of the perturbed pipe basic flow. The amplitude of the optimal perturbation on the basic flow rendering it linearly unstable is found to scale as $A_{cr} \sim Re^{-1}$. This is completely different from searching for the minimal finite perturbation destabilising a solution that, nevertheless, remains linearly stable, as is the case in our analysis.

7. Conclusion

The *streak breakdown* scenario has been shown to be a powerful mechanism of inducing transition to turbulence. It is, therefore, a good candidate to help to characterise the basin of attraction of the *Hagen-Poiseuille* flow. The critical amplitude threshold has been found to tend towards an exponential law of the Reynolds number with exponent $-3/2$, within the studied range.

The authors do not claim that the present computations prove an asymptotic behaviour of A_{cr}, as Re tends to infinity, of the form $A_{cr} \sim Re^{-3/2}$. Besides, the optimality of the chosen initial perturbation cannot be guaranteed from such a restricted exploration as we have performed. We envisage a computational study solving a problem closer to that of the experimental setup, with perturbations induced by a forcing extended in time, and compatible with the effects of the injection inflicted upon the experimental basic flow. We expect this will cast light on the reasons for the different behaviour observed. This study is under progress.

Acknowledgments

This work was supported by the Spanish Ministry of Science and Technology, grant FIS2004-01336.

References

[1] Boberg L and Brosa U 1988 Onset of turbulence in a pipe *Z. Naturforsch.* **43a** 697-726
[2] Schmid P J and Henningson D S 1994 Optimal energy growth in Hagen-Poiseuille flow *J. Fluid Mech.* **277** 197-225
[3] Zikanov O Y 1996 On the instability of pipe Poiseuille flow *Phys. Fluids* **8(11)** 2923
[4] Faisst H and Eckhardt B 2004 Sensitive dependence on initial conditions in transition to turbulence in pipe flow *J. Fluid Mech.* **504** 343-52
[5] Wedin H and Kerswell R R 2004 Exact coherent structures in pipe flow: travelling wave solutions *J. Fluid Mech.* **508** 333-71
[6] Brosa U and Grossmann S 1999 Minimum description of the onset of pipe turbulence *Eur. Phys. J. B.* **9** 343-54
[7] Hof B, Juel A and Mullin T 2003 Scaling of the turbulence transition threshold in a pipe *Phys. Rev. Lett.* **91(24)** 244502(4)
[8] Darbyshire A G and Mullin T 1995 Transition to turbulence in constant-mass-flux pipe flow *J. Fluid Mech.* **289** 83-114
[9] Meseguer A 2003 Streak breakdown instability in pipe Poiseuille flow *Phys. Fluids* **15(5)** 1203-13
[10] Priymak V G and Miyazaki T 1998 Accurate Navier-Stokes investigation of transitional and turbulent flows in a circular pipe *J. Comput. Phys.* **142** 370-411
[11] Meseguer A and Trefethen L N 2000 *A spectral Petrov-Galerkin formulation for pipe flow I: linear stability and transient growth*, Tech. Rep. 00/18, *Oxford University Comp. Lab.*
[12] Meseguer A and Trefethen L N 2003 Linearized pipe flow to Reynolds number 10^7 *J. Comput. Phys.* **186** 178-97
[13] Canuto C, Hussaini M Y, Quarteroni A and Zang T A 1988 *Spectral Methods in Fluid Dynamics* (Berlin: Springer)
[14] Cox S M and Matthews P C 2002 Exponential time differencing for stiff systems *J. Comput. Phys.* **176** 430-55
[15] Hairer E and Wanner G 1991 *Solving Ordinary Differential Equations. II. Stiff and Differential-Algebraic Problems* (Berlin: Springer)
[16] Pfenninger W 1961 *Boundary Layer and Flow Control* ed G V Lachman (New York: Pergamon) pp 970-980

[17] Chapman S J 2002 Subcritical transition in channel flows *J. Fluid Mech.* **451** 35-97
[18] Trefethen L N, Chapman S J, Henningson D S, Meseguer A, Mullin T and Nieuwstadt F T M 2000 *Threshold amplitudes for transition to turbulence in a pipe*, Tech. Rep. 00/17, *Oxford University Comp. Lab.*
[19] Draad A A, Kuiken G D C, and Nieuwstadt F T M 1998 Laminar-turbulent transition in pipe flow for Newtonian and non-Newtonian fluids *J. Fluid Mech.* **377** 267-312
[20] Gavarini M I, Bottaro A and Nieuwstadt F T M 2004 Laminar-turbulent transition in pipe flow for Newtonian and non-Newtonian fluids *J. Fluid Mech.* **517** 131-65